Low-dimensional model of a supersonic rectangular jet

D. Moreno,* A. Krothapalli,† M. B. Alkislar, and L. M. Lourenco
Department of Mechanical Engineering, Florida A&M University and Florida State University, 2525 Pottsdamer Street, Tallahassee, Florida 32310, USA

(Received 3 February 2003; revised manuscript received 11 August 2003; published 27 February 2004)

The proper orthogonal decomposition method is applied to the analysis of particle image velocimetry data obtained for a supersonic rectangular jet operated at underexpanded conditions. Phase-locked velocity field data were used to calculate the eigenfunctions and the eigenvalues. It was found that a large fraction of the total energy is contained within the first two modes. The essential features of the jet are thus captured with only two functions. A low-dimensional model for the dynamical behavior is then constructed using Galerkin projection of the isentropic compressible Navier-Stokes equations. The reduced model compares reasonably well with the experimental findings.

DOI: 10.1103/PhysRevE.69.026304 PACS number(s): 47.60.+i, 47.27.−i

I. INTRODUCTION

This paper is motivated by our attempt to provide a method of velocity field data analysis aimed at obtaining low-dimensional approximate description of high speed jets. The velocity field data is obtained experimentally using the particle image velocimetry (PIV) technique. Recent developments in the statistical technique of proper orthogonal decomposition (POD) seems to offer some hope to capture the spatial as well as temporal behavior of energetic large-scale structures in a variety of turbulent shear flows. Data analysis using POD is often conducted to extract ''mode shapes'' or basis functions from experimental data for subsequent use in Galerkin projections that yield low-dimensional models [1]. This enables one to build efficient reduced order models based on the first few dynamically important POD modes, thus serving as potential substitute for computationally intensive simulations.

The POD method was originally suggested by Lumely [2] to extract organized large-scale structures from turbulent flows. The method provides a set of optimized orthonormal basis functions for an ensemble of data. The most important property of POD is its optimality in the sense that it provides the most efficient way of capturing the dominant features of an infinite-dimensional process with only few functions.

Since the introduction of POD as a tool to extract coherent structure in turbulent flows, many studies on the subject have been published. The method has proved to be a powerful tool in educing coherent structures. It has been applied to many kinds of flows such as, boundary layers [3,4], bounded flows [5–7], shear layers [8–10], turbulent jets [11–17], and compressible flows [18,19]. In most of these cases, it has been found that few modes contain a high percentage of the energy. It is important to point out that these flows have been mostly at subsonic velocities and the information is limited due to coarse spatial resolution of the velocity measuring sensors (hot-wire probes). As a result, the velocity field generally yields few modes, which contain most of the energy. However, with direct numerical simulation, it is possible to resolve spatially a great number of scales within the region of interest. But the flows analyzed have been at low Reynolds numbers [4,7,19]. On the other hand, using whole field techniques such as laser induced fluorescence, interferometry tomography, and PIV, it is possible to obtain data with high spatial resolution at high Reynolds numbers. In these cases, the POD method has shown energy distributed among larger number of modes [14–16], since many scales are captured in an instantaneous flow field. Most of the previous investigations have developed low-dimensional order model using Galerkin projection and the flows studied have been in the incompressible regime [3,4,10,18,20]. The only exception is the work of Rowley *et al.* [19], which dealt with compressible flows at subsonic Mach numbers.

In the present study, POD method is applied to PIV data set that was obtained from the phase-locked measurements of synoptic velocity field of an underexpanded rectangular jet. The screeching jet is dominated by coherent large-scale structures generated by the inherent global instability set up by a feedback mechanism [21–23]. The feedback cycle starts with a disturbance in the shear layer that is convected downstream and come in contact with shock cell boundary. This interaction, particularly at the end of the shock cell, produces intense sound wave. This sound wave propagates upstream in the ambient medium, interacts with the incipient shear layer at the nozzle exit and produces a new downstream traveling disturbance that continues the feedback cycle.

It is an attempt in our endeavor in providing a low order dynamic model suitable to predict the main characteristics of supersonic jets. In this paper we will apply the technique to describe the structure of a screeching rectangular jet.

II. THEORETICAL BACKGROUND

A. Brief remarks on the POD method

In the present study, the procedure outlined in Berkooz *et al.* [24] is followed. The idea behind POD is to find a basis function $\{\varphi\}$ in which the ensemble data $\{\mathbf{u}\}$ is optimally represented. In this paper, $\mathbf{u}$ is considered a real random vector of length M with temporal and spatial dependence. Thus, we are looking for a function that maximizes the inner product with $\mathbf{u}$, which is given as

*Present address: Centro de Investigaciones en Optica A.C., Mexico.
†Electronic address: kroth@eng.fsu.edu

$$\max_{\boldsymbol{\varphi}} \frac{\overline{|(\mathbf{u},\boldsymbol{\varphi})|^2}}{\|\boldsymbol{\varphi}\|^2}, \tag{1}$$

where (,) represents the inner product in the Hilbert space of square integrable functions, $\|\ \|$ is the corresponding norm, and the overbar represents an ensemble average in time. Solution of Eq. (1) is a problem of calculus of variations [25] and it can be represented as

$$\int \int_D \mathbf{R}_{ij}(\mathbf{x},\mathbf{x}')\boldsymbol{\varphi}_j^{(n)}(\mathbf{x}')\mathbf{dx}' = \lambda^{(n)}\boldsymbol{\varphi}_i^{(n)}(\mathbf{x}), \tag{2}$$

where D is the two-dimensional domain of the velocity field and the kernel R is the average autocorrelation function defined by

$$R(x,x') = \overline{u_i(x)u_j^*(x')} \tag{3}$$

The symbol * corresponds to the complex conjugate.

The solution of Eq. (2) represents a set $\boldsymbol{\varphi}^{(n)}$ of basis functions with special properties attractive for the purpose of deriving dynamical equations via Galerkin projection. The eigenfunctions form an orthogonal system, which can be normalized as

$$(\boldsymbol{\varphi}^m,\boldsymbol{\varphi}^n) = \delta_{mn}\lambda_n, \tag{4}$$

where δ_{mn} is the Kronecker delta symbol. The system $\boldsymbol{\varphi}^{(n)}$ is complete in the sense that velocity field $\mathbf{u}$ is represented as expansion of orthogonal eigenfunctions

$$\mathbf{u}(\mathbf{x},t_k) = \sum_{n=1}^{N} \zeta^n(t_k)\boldsymbol{\varphi}^{(n)}(\mathbf{x}), \tag{5}$$

where ζ is the dot product for $\mathbf{u}$ and $\boldsymbol{\varphi}^{(n)}$, that is, ζ is the projection of $\mathbf{u}$ in the direction represented by $\boldsymbol{\varphi}^{(n)}$. An important property of eigenfunction $\boldsymbol{\varphi}^{(n)}$ is that it can be expanded as a linear combination of the instantaneous velocity fields as

$$\boldsymbol{\varphi}(\mathbf{x}) = \sum_{k=1}^{M-1} A_k\mathbf{u}(\mathbf{x},t_k), \tag{6}$$

where the eigenfunction $\boldsymbol{\varphi}$ possesses the properties of the velocity field.

In this work the data used are velocity field realizations of 83×136 vectors and hence a vector length of 11 288. The corresponding autocorrelation matrix has dimensions of $11\,288\times11\,288$. The solution of the eigenvalue problem for such a large matrix is quite cumbersome and very time consuming with the current computers. Sirovich [1] proposed an equivalent approach to overcome this difficulty in which R_{ij} can be expressed as

$$\mathbf{R}_{ij}(\mathbf{x},\mathbf{x}') = \frac{1}{M}\sum_{n=1}^{M} u_i^n u_j^n. \tag{7}$$

Here, M is the number of snapshots (or realizations).

If Eqs. (2), (6), and (7) are combined, the following is obtained

$$\mathbf{CA} = \lambda\mathbf{C}, \tag{8}$$

where $\mathbf{C}$ is an $M\times M$ matrix defined as

$$C_{mn} = (u_m,u_n). \tag{9}$$

B. Galerkin projection

We are now interested in deriving dynamical equations for the evolution of the expansion coefficients $\zeta(t)$ in time. A common process is the method of Galerkin projection. The Galerkin method is a discretization scheme for partial differential equations (PDE's), which is generically categorized as one of the spectral methods or methods of weighted residuals. This method is based on the separation of variables approach and is an attempt to find an approximate solution in the form of truncated series expansion given by

$$\mathbf{u}(\mathbf{x},t_k) = \sum_{n=1}^{N} \zeta^{(n)}(t_k)\boldsymbol{\varphi}^{(n)}(\mathbf{x}). \tag{10}$$

Here, $\boldsymbol{\varphi}^{(n)}$ are known eigenfunctions calculated using the POD method described earlier. Thus, the original infinite-dimensional system is approximated by a N-dimensional system, where the order of the reduced model is determined by the truncation velocity $\mathbf{u}$. The method then involves the projection of the truncated velocity represented by Eq. (5) on to the Navier-Stokes (N-S) equations. A brief description of this procedure is given below.

Suppose we have a system governed by the PDE's

$$\frac{\partial\mathbf{u}}{\partial t} = D(\mathbf{u}), \quad \mathbf{u}:D\times(0,\infty)\rightarrow\mathbf{R}, \tag{11}$$

with appropriate boundary conditions and initial conditions, where $D(\ )$ is a spatial operator. On projecting the eigenfunctions, φ^n on to Eq. (11), the following expression is obtained:

$$\left(\boldsymbol{\varphi}^{(n)},\left(\frac{\partial\mathbf{u}}{\partial t} - D(\mathbf{u})\right)\right) = 0, \quad n = 1,...,M. \tag{12}$$

The operation above leads to a set of ordinary differential equations of the form

$$\frac{d\zeta^{(n)}}{dt} = F_i(\zeta^1,\ldots,\zeta^M), \tag{13}$$

where $\zeta = (\zeta^1,\ldots,\zeta^M)$ and $F:\mathbf{R}^N\rightarrow\mathbf{R}^N$. By solving the reduced order model represented by Eq. (13) and substituting back into Eq. (10) we get an approximate solution for $\mathbf{u}(\mathbf{x},t)$. This procedure will avoid solving the infinite-dimensional system given by the original PDE's and it provides a practical procedure for studying the evolution of the flow field in time.

C. Equations of motion

The method developed by Rowley *et al.* [19] is followed for applying scalar-valued POD/Galerkin to compressible

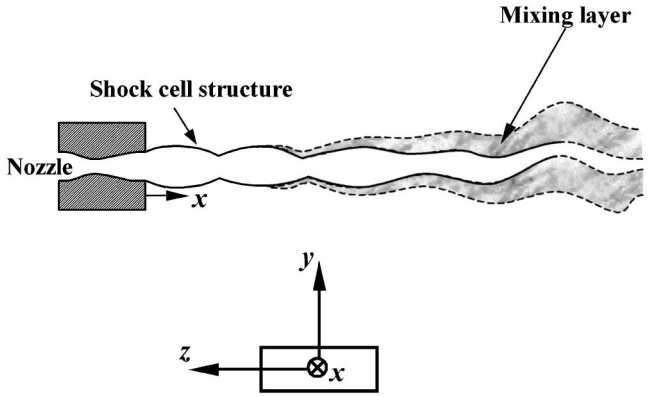

FIG. 1. A Cartesian coordinate system and general features of the supersonic jet.

flows using the isentropic N-S equations. Since, the original compressible equations are quite complicated, approximations are made to obtain a simpler set of equations that can be used for Galerkin projection. The detailed derivation of the equations can be found in Rowley *et al.* [26]. The resulting equations of motion in nondimensional form are

$$u_t+uu_x+vu_y+\frac{1}{M^2}\frac{2}{\gamma-1}aa_x=\frac{1}{\mathrm{Re}_h}(u_{xx}+u_{yy}),$$

$$v_t+uv_x+vv_y+\frac{1}{M^2}\frac{2}{\gamma-1}aa_y=\frac{1}{\mathrm{Re}_h}(v_{xx}+v_{yy}),$$

$$a_t+ua_x+va_y+\frac{\gamma-1}{2}a(u_x+v_y)=0, \tag{14}$$

where a is the local sound speed, $\gamma=1.4$ is the specific heat coefficient, and $\mathrm{Re}_h=U_jh/\nu$ is the Reynolds number with ν as the kinematic viscosity. Velocities have been normalized by the fully expanded jet velocity U_j, a is normalized by the ambient sound speed a_0, x and y by the nozzle height h, and time by h/U_j.

In order to apply Galerkin projection to the phase resolved experimental data, the velocity and speed of sound in Eq. (14) were decomposed by the method followed by Reynolds and Hussein [27]. Any time variable f describing a parameter of an oscillating flow can be defined as a composition of a mean, a periodic, and a random component, as given below

$$f=\overline{f}+\tilde{f}+f', \tag{15}$$

where $\overline{f}$ is the global mean, $\tilde{f}$ and f' are the periodic mean and random component, respectively. The experimental data were taken at several phases of a screech cycle. The phase-averaged component is given by the following expression:

$$\langle f\rangle=\overline{f}+\tilde{f}, \tag{16}$$

where $\langle\ \rangle$ is the phase average. The POD method is applied to the periodic component $\tilde{f}$ and it can be represented in terms of eigenfunctions $\varphi^{(n)}$ and time coefficients $\zeta^{(n)}$ as

$$\tilde{f}=\sum_{n=1}^{M}\zeta^{(n)}(t_k)\varphi^{(n)}(x). \tag{17}$$

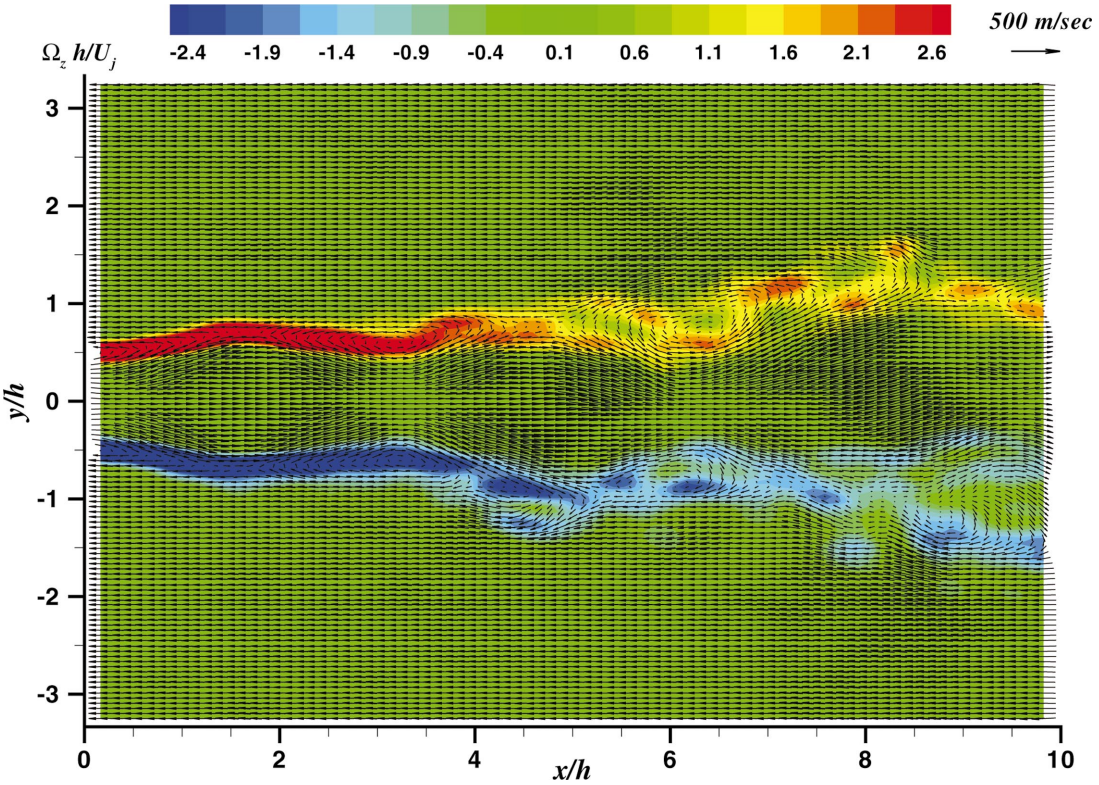

FIG. 2. (Color) A typical instantaneous flow field.

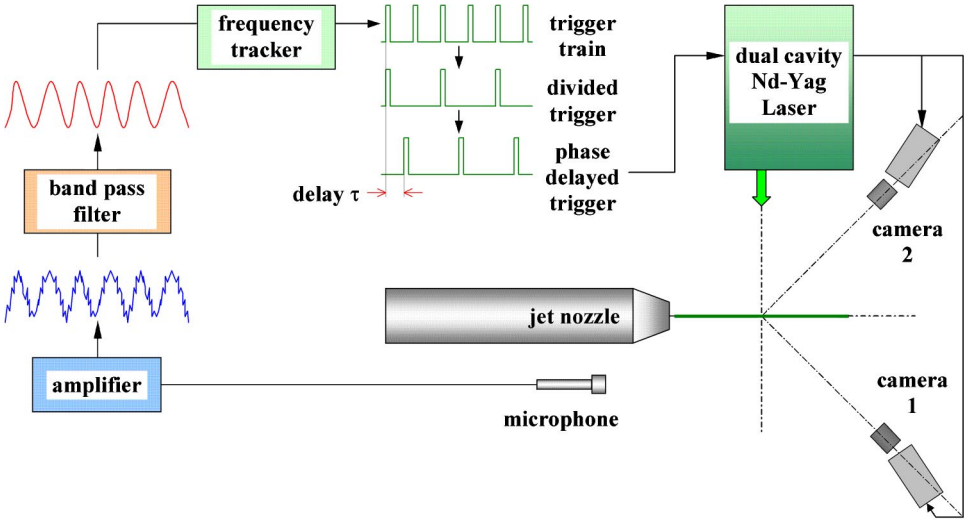

FIG. 3. Illustration of phase-locked system for stereoscopic PIV measurements cycle.

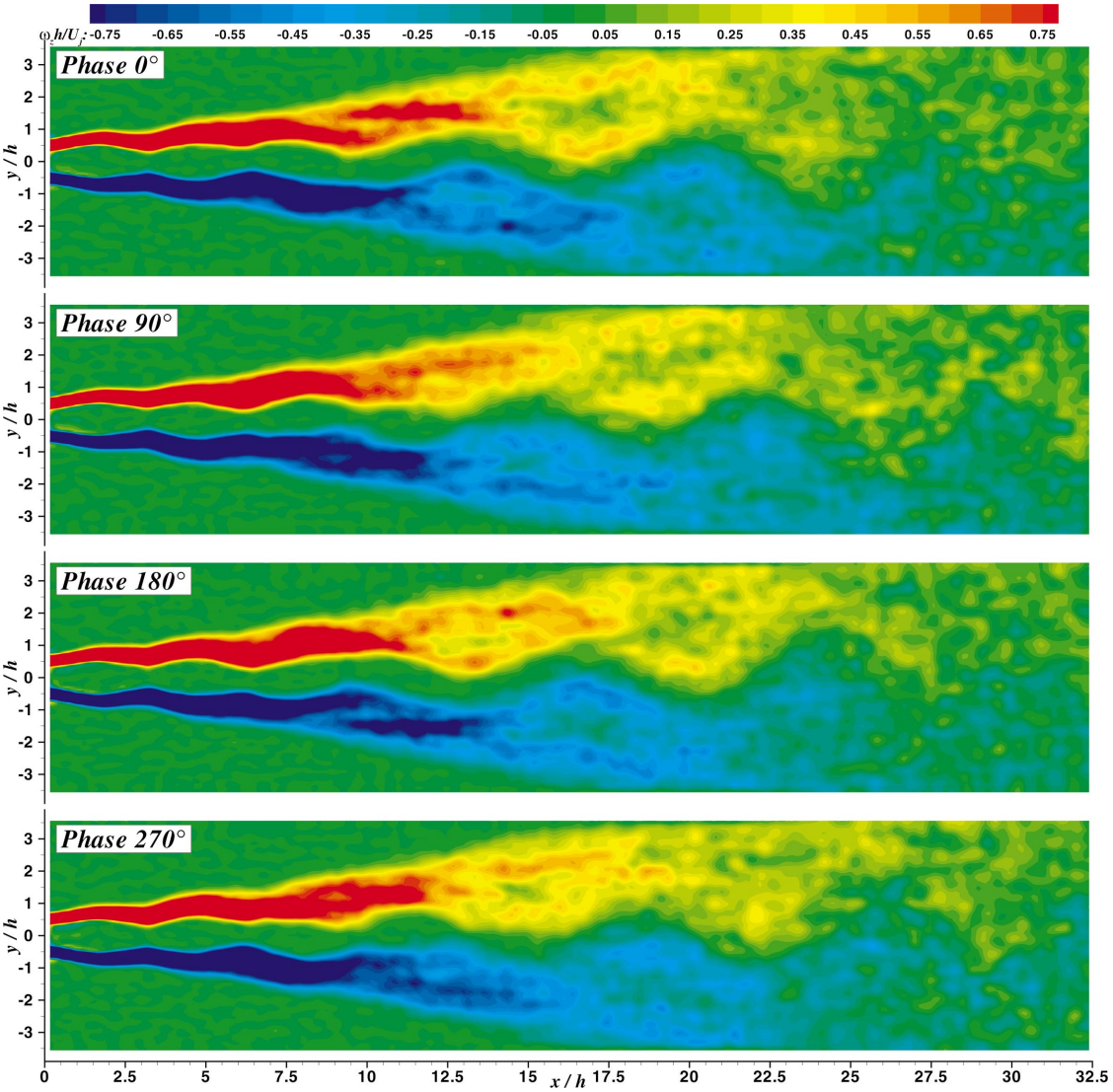

FIG. 4. (Color) Phase-locked vorticity field at four consecutive phases within the screech cycle.

TABLE I. The first 10 eigenvalues (energy represented in percent of the total energy).

i	$\lambda_{(u)}$	$\lambda_{(v)}$	$\lambda_{(\omega_z)}$
1	45.87	57.41	39.91
2	35.43	32.00	29.76
3	4.33	1.70	4.13
4	2.66	1.44	3.25
5	2.06	1.18	3.15
6	1.57	0.92	2.40
7	1.34	0.89	2.40
8	1.20	0.86	2.19
9	1.07	0.69	2.14
10	0.96	0.57	2.03

Following the decomposition given in Eq. (15), the velocity and speed of sound can be written as

$$\mathbf{u}=\overline{\mathbf{u}}+\tilde{\mathbf{u}}+\mathbf{u}',$$

$$a=\overline{a}+\tilde{a}+a'. \tag{18}$$

In order to obtain the equations of motion for the periodic mean components, first the decomposed variables in Eq. (18) were substituted in Eq. (14). Then, the resulting equation set is averaged separately in phase and time. Finally the time averaged equations are subtracted from the phase-averaged equations to obtain the equations of motion for the periodic mean components as in Eq. (19). The detailed procedure of this derivation can be found in Reynolds and Hussein [27].

$$\begin{aligned}
&\tilde{u}_t+\overline{u}\tilde{u}_x+\tilde{u}\overline{u}_x+\overline{v}\tilde{u}_y+\tilde{v}\overline{u}_y+\tilde{u}\tilde{u}_x-\overline{\tilde{u}\tilde{u}_x}+\langle u'u'_x\rangle-\overline{u'u'_x}\\
&\quad+\tilde{v}\tilde{u}_y-\overline{\tilde{v}\tilde{u}_y}+\langle v'u'_y\rangle-\overline{v'u'_y}+\frac{1}{M^2}\frac{2}{\gamma-1}(\overline{a}\tilde{a}_x+\tilde{a}\overline{a}_x\\
&\quad+\tilde{a}\tilde{a}_x-\overline{\tilde{a}\tilde{a}_x}+\langle a'a'_x\rangle-\overline{a'a'_x})=\frac{1}{\mathrm{Re}_h}(\tilde{u}_{xx}+\tilde{u}_{yy}),\\
&\tilde{v}_t+\overline{u}\tilde{v}_x+\tilde{u}\overline{v}_x+\overline{v}\tilde{v}_y+\tilde{v}\overline{v}_y+\tilde{u}\tilde{v}_x-\overline{\tilde{u}\tilde{v}_x}+\langle u'v'_x\rangle-\overline{u'v'_x}\\
&\quad+\tilde{v}\tilde{v}_y-\overline{\tilde{v}\tilde{v}_y}+\langle v'v'_y\rangle-\overline{v'v'_y}+\frac{1}{M^2}\frac{2}{\gamma-1}(\overline{a}\tilde{a}_y+\tilde{a}\overline{a}_y\\
&\quad+\tilde{a}\tilde{a}_y-\overline{\tilde{a}\tilde{a}_y}+\langle a'a'_y\rangle-\overline{a'a'_y})=\frac{1}{\mathrm{Re}_h}(v_{xx}+v_{yy}),\\
&\tilde{a}_t+\overline{u}\tilde{a}_x+\tilde{u}\overline{a}_x+\overline{v}\tilde{a}_y+\tilde{v}\overline{a}_y+\tilde{u}\tilde{a}_x-\overline{\tilde{u}\tilde{a}_x}+\langle u'a'_x\rangle-\overline{a'a'_x}\\
&\quad+\tilde{v}\tilde{a}_y-\overline{\tilde{v}\tilde{a}_y}+\langle v'a'_y\rangle-\overline{v'a'_y}+\frac{\gamma-1}{2}(\overline{a}\tilde{u}_x+\tilde{a}\overline{u}_x+\overline{a}\tilde{v}_y\\
&\quad+\tilde{a}\overline{v}_y+\tilde{a}\tilde{u}_x-\overline{\tilde{a}\tilde{u}_x}+\langle a'u'_x\rangle-\overline{a'u'_x}+\tilde{a}\tilde{v}_y-\overline{\tilde{a}\tilde{v}_y}\\
&\quad+\langle a'v'_y\rangle-\overline{a'v'_y})=0.
\end{aligned} \tag{19}$$

In Eq. (19), the periodic Reynolds stresses $-\overline{\tilde{u}_i\tilde{u}_j}$ are the terms involving the periodic motion. Those terms make the equation different from the usual Reynolds average equation for turbulent flow and give the effect of the oscillation on the mean flow.

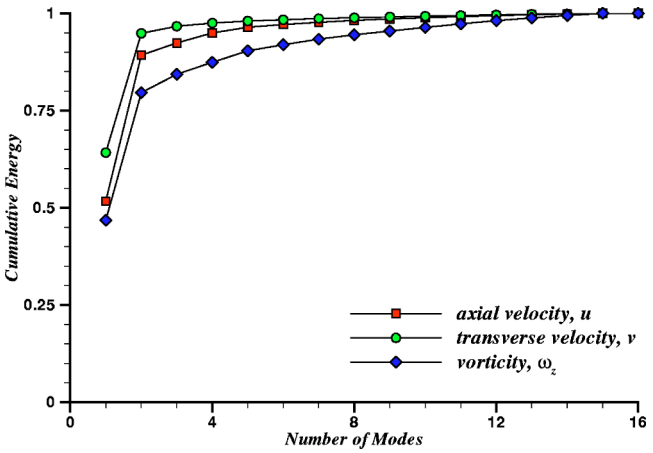

FIG. 5. POD cumulative energy distribution.

Substituting Eq. (17) in Eq. (19) and applying Galerkin projection, the following equation is obtained in vector form:

$$\mathbf{A}_t=\mathbf{B}+\mathbf{C}+\mathbf{D}+\mathbf{E}+\mathbf{F}+\mathbf{G}+\mathbf{H}, \tag{20}$$

where

$$A=\{\zeta_k^u,\zeta_k^v,\zeta_k^a\},$$

$$B=\{b_k^u,b_k^v,b_k^a\},$$

$$C=\{c_{ik}^u,c_{ik}^v,c_{ik}^a\}\zeta_i^u,$$

$$D=\{d_{ik}^u,d_{ik}^v,d_{ik}^a\}\zeta_i^v,$$

$$E=\{e_{ik}^u,e_{ik}^v,e_{ik}^a\}\zeta_i^a,$$

$$F=\{f_{ijk}^u\zeta_j^u,f_{ijk}^v\zeta_j^v,f_{ijk}^a\zeta_j^a\}\zeta_i^u,$$

$$G=\{g_{ijk}^u\zeta_j^u,g_{ijk}^v\zeta_j^v,g_{ijk}^a\zeta_j^a\}\zeta_i^v,$$

$$H=\{h_{ijk}^u,h_{ijk}^v\}\zeta_{ij}^a.$$

In these expressions, b contains terms involving Reynolds stresses that were obtained directly from experimental data, and c, d, e, f, g, and h are constant parameters determined by using calculated eigenfunctions in the preceding section.

III. EXPERIMENTAL APPARATUS AND PROCEDURES

Experiments were conducted in the blow-down jet facility of the Fluid Mechanics Research Laboratory [28]. This facility is capable of generating jets with Reynolds numbers in excess of 3×10^6 with exit Mach numbers up to 2.15 and total temperatures up to 800 K. The $M_d=1.44$, convergent-divergent nozzle used in this study has a rectangular exit with 4:1 aspect ratio and 10 mm in short dimension (h).

The mean exit velocity profile with laminar boundary layers was top hat as the jet was exhausted into a quiet surrounding at ambient conditions. The jet exit Reynolds num-

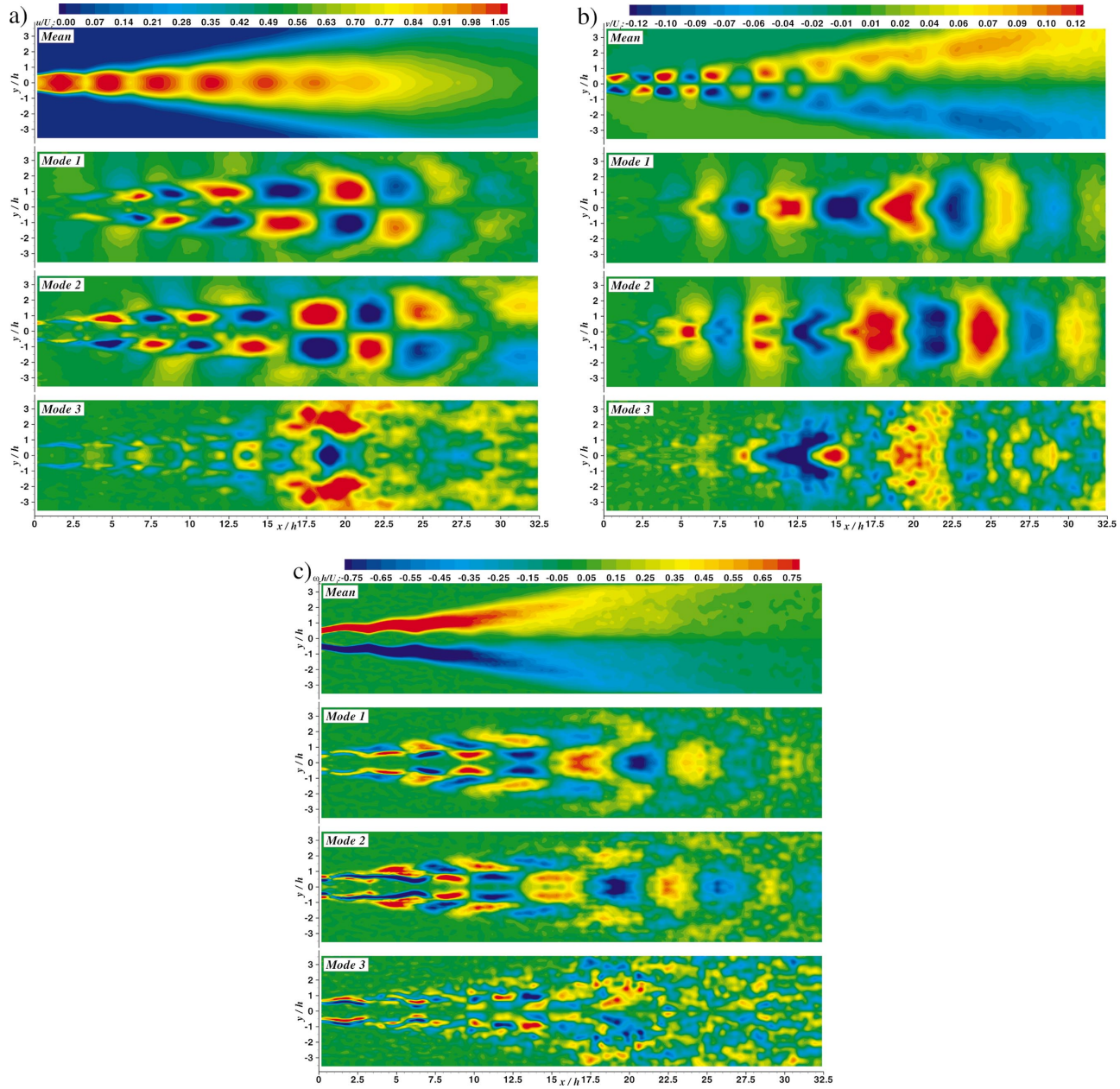

FIG. 6. (Color) Average and first three modes of (a) axial velocity, (b) transverse velocity, and (c) vorticity.

ber based on the nozzle exit height and the mean exit velocity is 3.3×10^5. A Cartesian coordinate system (X,Y,Z) was chosen with its origin located at the center of the nozzle exit plane and with X axis oriented along the centerline of the jet, Y and Z axes are oriented along the short and long dimensions, respectively (Fig. 1). The measurements are confined to the central plane (XY plane) of the jet containing the small dimension of the nozzle. Because of the slender character of the jet flow, it is necessary to cover the entire jet in several measurement zones. These zones may have different sizes to cover the regions of interest. In addition, they overlap on each other to ensure the coverage of the whole field and for a proper match.

Nonintrusive measurements of the velocity field were made using stereoscopic PIV. A detailed discussion of the application of the stereoscopic PIV technique to supersonic jets is given in Alkislar [28–30]. The flow was seeded internally with submicron particles generated by a modified Wright nebulizer in the size range of 0.1–1 μm. Rosko fog generator was used to seed the ambient air with particle sizes 1–10 μm.

A typical instantaneous velocity field obtained in the central plane containing the small dimension of the nozzle, covering the region from the nozzle exit to about $10h$, is shown in Fig. 2. The uniformly scaled velocity vectors superimposed with the contours of the out of plane component of the vorticity are also shown in the figure. The convective velocity of vortical structures is subtracted from the whole velocity field to show the details of the shear layer. The data was obtained using an 83×136 (X,Y) Cartesian grid. The jet was

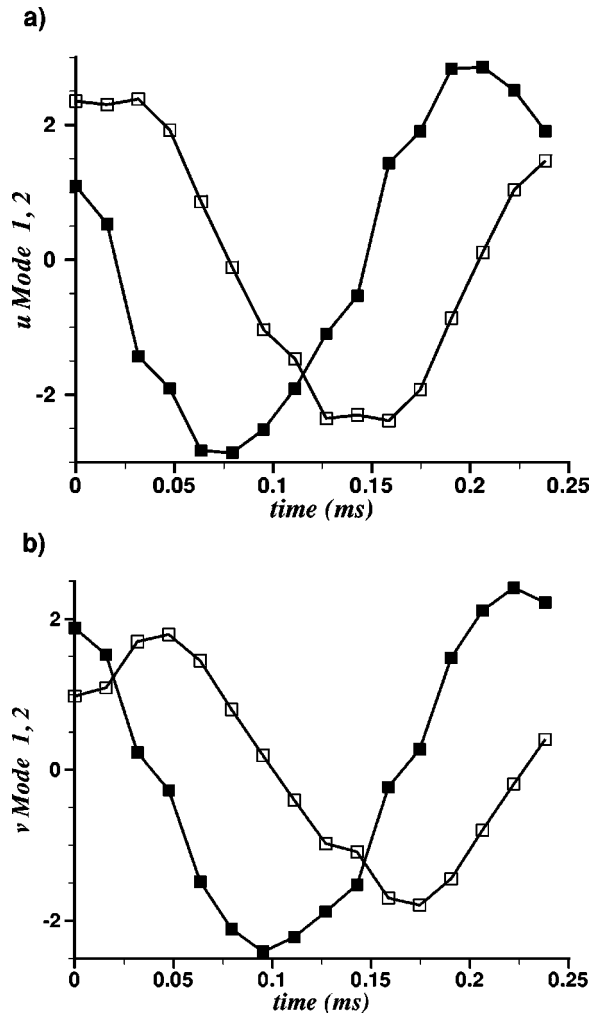

FIG. 7. Time coefficients for mode 1 (filled square) and 2; (a) axial, (b) transverse velocity.

operated at the underexpanded jet condition corresponding to the fully expanded jet Mach number of 1.69. The jet displays organized vortical structures that are generated by the well known feedback mechanism. The large structures in screeching jets typically appear at a periodic rate, giving rise to the opportunity of acquiring the phase-locked velocity field data.

The near field microphone signal is used for the timing reference for the phase averaging of the PIV data at specific phases of the driving signal as illustrated in Fig. 3. Corresponding to each phase, there is a composite snapshot of the flow field starting at some reference time given by the microphone signal. The composite snapshots approximate reasonably the instantaneous flow field for the purposes of extracting the large-scale coherent vortical structures in the jet. PIV results suggest that 30 samples are sufficient to achieve statistical convergence of the velocity field at constant phase. The data was sampled at 22.5° intervals within the first half of the screech cycle. It was found that the selected data taken in the second half of the screech cycle was simply a reflection of the data. In total 560 instantaneous velocity fields are obtained. The details of the phase-locked system are given in Alkislar [28].

IV. RESULTS AND DISCUSSIONS

The global mean velocity of the flow is first obtained using 560 instantaneous velocity fields. The periodic velocity field is then obtained from subtracting the global mean from each of the phase-averaged velocity fields. The periodic velocity field realizations are used to compute the eigenvalues and eigenfunctions using the method outlined in Sec. II A. The data covers the region $x/h=0.1-32.4$. At each phase, 35 realizations are considered. Sixteen phases within the screech cycle are used. The mean vorticity at constant phase is calculated using the expression

$$\langle \omega_z \rangle = \frac{\partial \langle v \rangle}{\partial x} - \frac{\partial \langle u \rangle}{\partial y}. \tag{21}$$

The contours of the normalized vorticity magnitude at four different phases within a screech cycle are shown in Fig. 4. The vorticity contours seen in the figure are a clear indication of the presence of large-scale coherent vortical structures. The large vortical structures are convected downstream at half the jet exit velocity. They appear at a periodic rate at a frequency of 4200 Hz. The vortical structures are highly three dimensional in nature and as a result, the vorticity contours appear to be fragmented. The source of three dimensionality can be attributed to the generation of streamwise vortices in the shear layers [21]. The periodic shock cell structure commonly seen in underexpanded jets is also evident in this figure. More detailed description of the large-scale structure dynamics for this flow is given in Alkislar [30].

A. Energy distribution

The energy associated with different eigenfunctions is contained in their corresponding eigenvalue λ. In Eq. (9), **C** is a real symmetric matrix, it has positive real eigenvalues, and **A** can be structured in decreasing order of the corresponding eigenvalues $\lambda^1>\lambda^2>,\ldots,\lambda^n>0$. The relative values of λ^n reflect the amount of energy in each eigenfunction (or mode), that is,

$$E_n = \frac{\lambda_n}{\Sigma_{n=1}^{M} \lambda_n} \tag{22}$$

is a fraction of the data set energy that is contained in the direction of the nth eigenfunction φ.

Table I lists the relative energy of the eigenvalues for the first 10 modes for the axial and transverse components of the velocity and the corresponding vorticity fields. The cumulative energy of the eigenvalues is shown in Fig. 5. It is observed from the data that the first two modes contain significant percent of the total energy. Accordingly, the analysis of the mode shapes to be discussed later is confined mostly to these dominant modes.

In the context of fluid mechanics problems, it has been suggested that a 99% of the total energy be used as cutoff for representing the flow field accurately [1]. On the other hand, Palacios [31] suggests that 75% of the energy may be sufficient for a good representation of the system. In the present study, to quantify the accuracy of the reconstructed phase-averaged flow field, the mean square error in the velocities

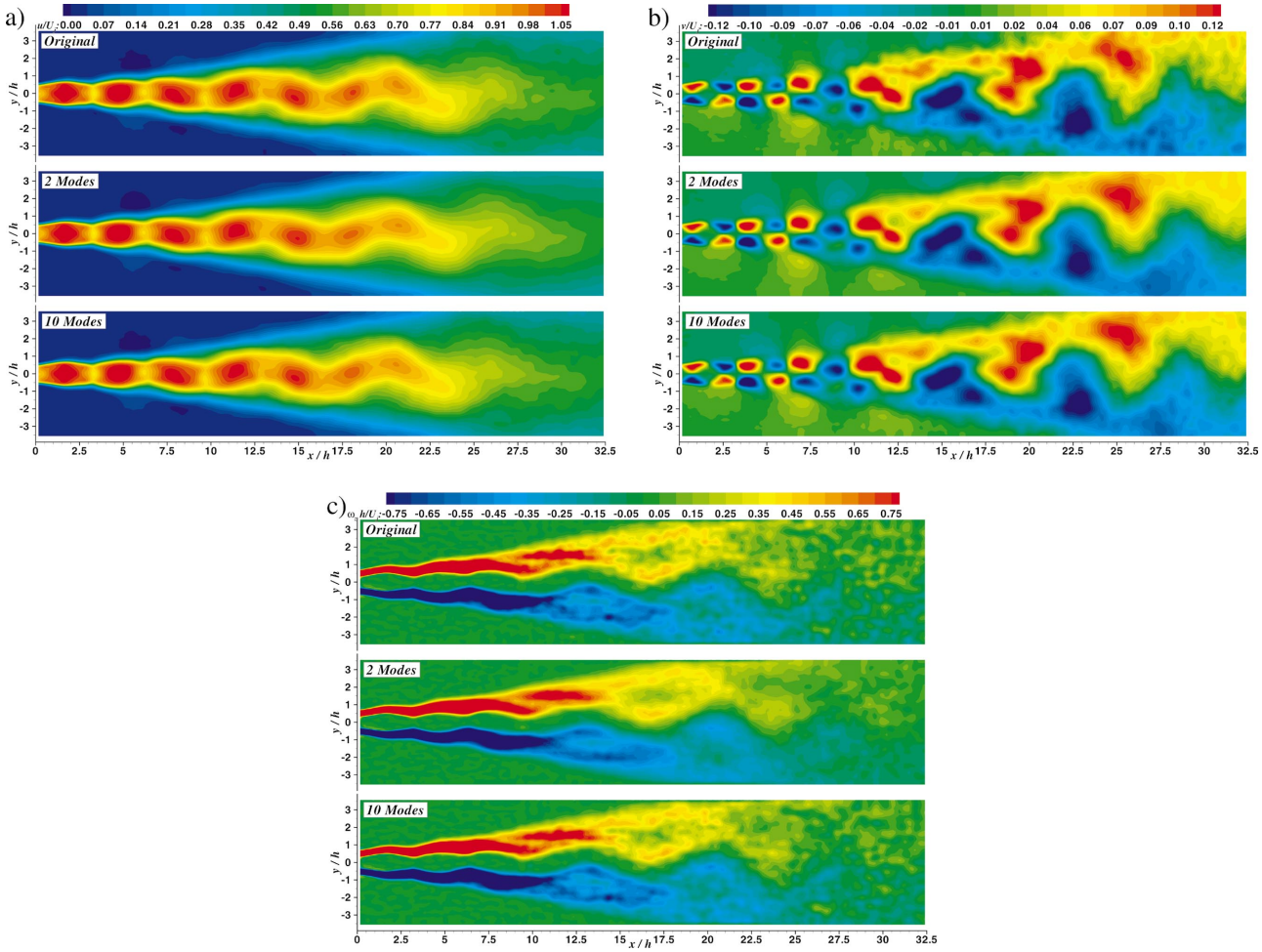

FIG. 8. (Color) The comparison of original flow field with POD reconstructions. (a) Axial velocity, (b) transverse velocity, and (c) vorticity.

was calculated. Considering only two modes, which correspond to 90% of the total energy, the mean square error is found to be 0.03% for the axial and 1.2% for the transverse velocities. Hence, the reconstructed flow field using two modes is a good representation of the flow field.

B. Mode shapes and reconstruction

The characteristics of the POD modes are now examined to understand the large-scale structure dynamics. Figure 6 presents the first three mode shapes corresponding to the axial velocity, transverse velocity, and the vorticity. Also included in the figure are their experimentally determined global mean distributions. The color contours in the figure representing the mode shapes have both positive (red) and negative (blue) values. The mode shapes are simply a pattern that may not provide a direct connection to the large-scale structure physics. However, upon close examination, it is observed that the peak magnitude locations in the first two mode shapes appear to coincide with the corresponding peak periodic Reynolds stresses [26]. Hence, it is believed that the mode shape structure may have some relationship with coherent structure dynamics.

It is interesting to observe that the eigenvalues occur in a pair of almost equal value, whereas there is a large gap in magnitude between this pair of eigenvalues and the next ones. The same observation was also made by Rempfer [4], Rajaee *et al.* [10], and Rowley *et al.* [19]. Figures 6 and 7 show clearly the reason for this behavior. For the axial and transverse velocities mode shapes 1 and 2 are nearly identical, where mode 2 shifted in the streamwise direction by approximately one quarter-wavelength in space and the corresponding time coefficients are analogously phase shifted in time by $\pi/2$. It is known that structures represented by the eigenfunctions are fixed in space. However, when one mode, in the pair, is in the maximum energy stage the other is in the minimum energy stage, and this relation reverses after one quarter of a period in time, that is, the energy is exchanged between the two modes thereby propagating the flow pattern consisting of the sum of the two in the positive streamwise direction.

Using the dominant POD mode shapes, the velocity and vorticity fields at a constant phase are reconstructed as shown in Fig. 8. Reconstruction is carried out using Eq. (5). The original experimental data at the corresponding phase is also included in the figure for comparison. From the reconstructed data, it appears that the first two modes capture the velocity and vorticity fields with fidelity. The flow reconstruction using more than the first two modes appears to add

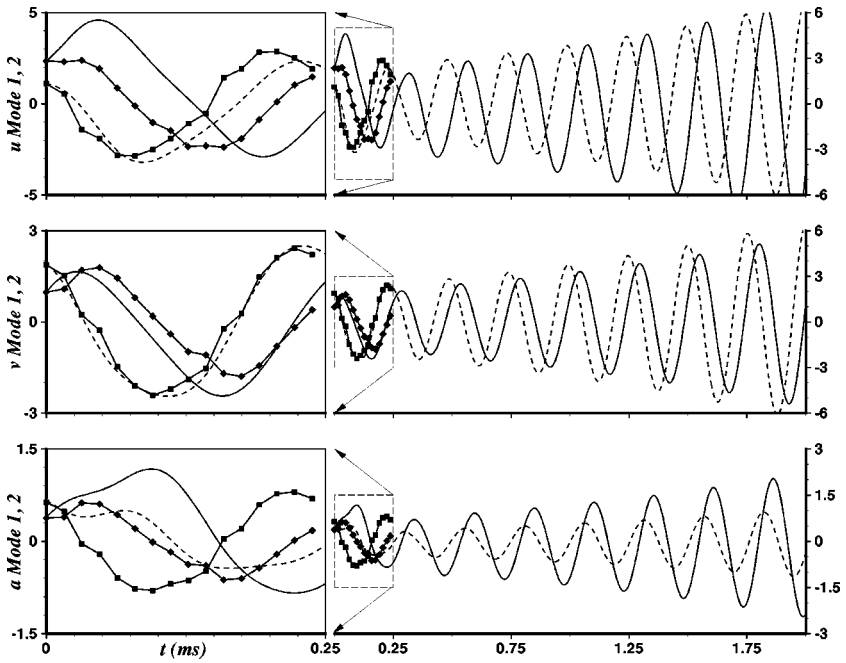

FIG. 9. Time traces of first 2 modes for axial velocity, transverse velocity, and sound speed at $x/h=0-10$. Experimental: symbol, "■" first mode and "◆" second mode. Galerkin prediction, "--" first mode, and "···" second mode.

little information. Therefore, the two energetic modes are sufficient to capture the complete structure of the flow within the region where the large structure dynamics are most important. Based on this observation, the two dominant modes are used in the low-dimensional modeling using the above-described Galerkin procedure.

C. Low order modeling

The scalar-valued POD/Galerkin method is applied to predict the flow field using computed eigenfunctions from POD analysis. The speed of sound has been calculated approximately, through the temperature $\overline{T}$, by using the Crocco's relationship [32] which is valid for a boundary layer flow with a Prandtl number Pr=1 and constant pressure

$$\frac{\overline{T}}{T_0}=\frac{T_\infty}{T_0}+\left(1+\frac{T_\infty}{T_0}\right)U_c+(\gamma-1)M^2U_c\frac{(1-U_c)}{2}, \quad (23)$$

where T_∞ is the ambient temperature, U_c is the center line

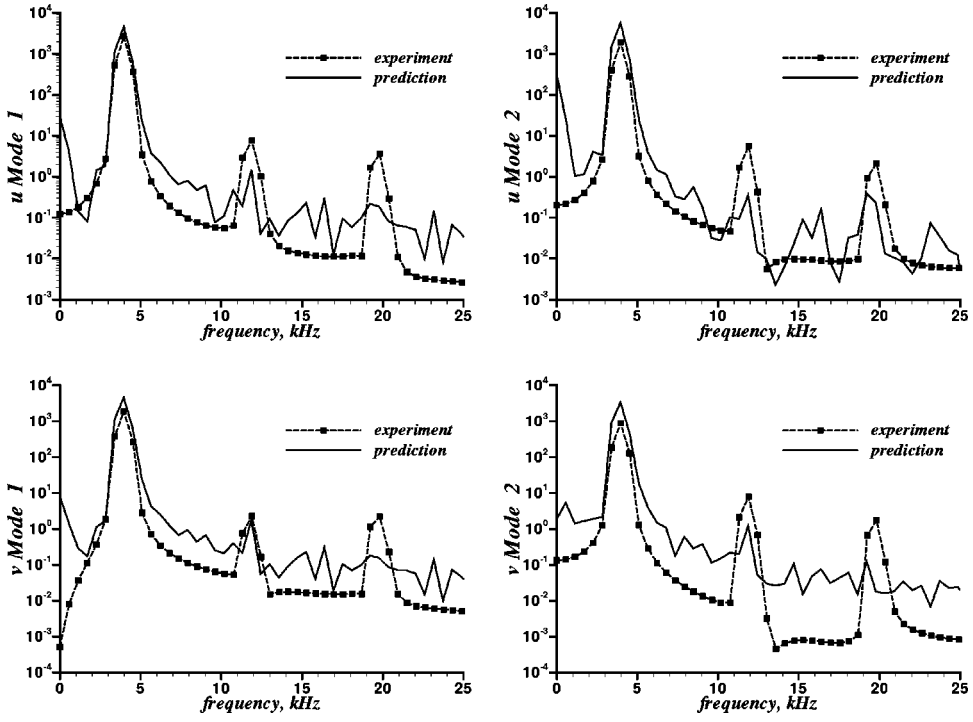

FIG. 10. Comparison of spectrums of the time traces of "■" experimental and "-" Galerkin prediction results.

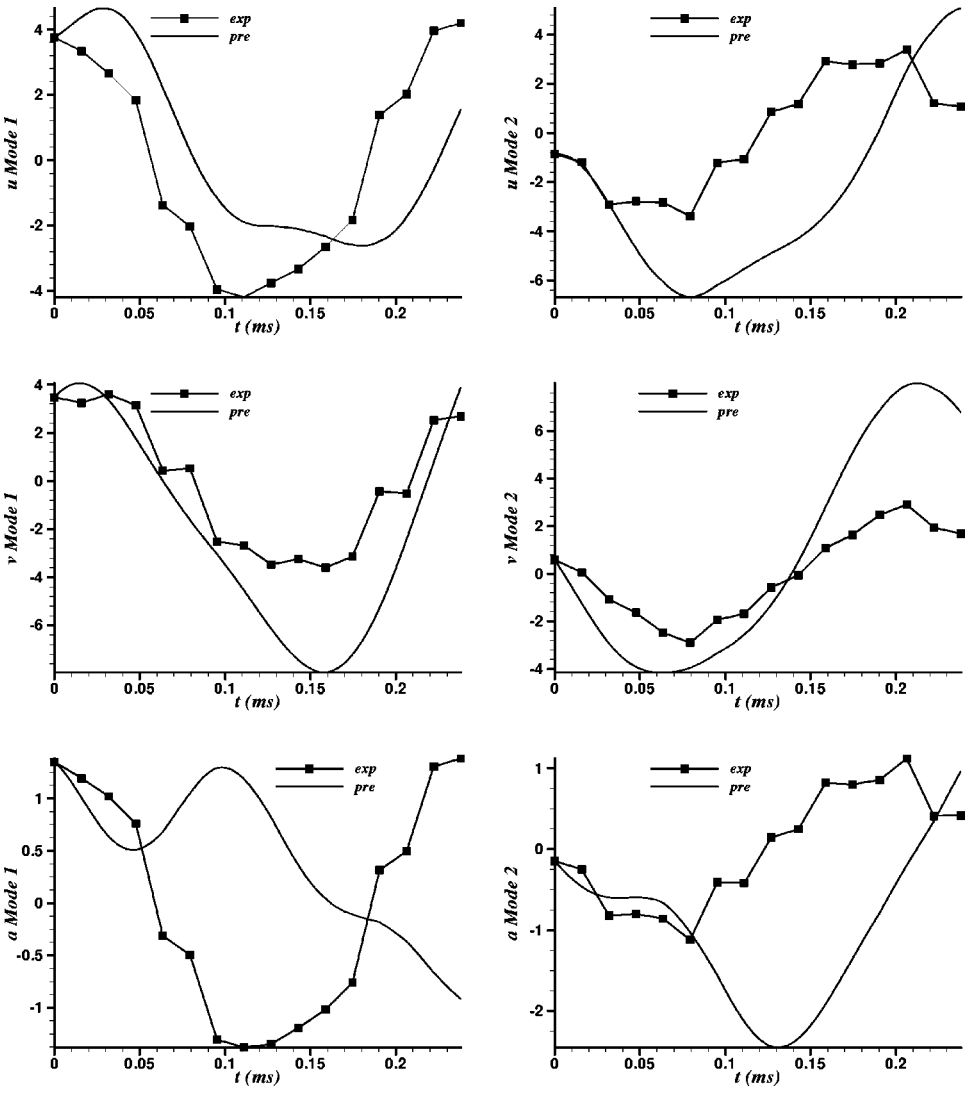

FIG. 11. Time traces of first 2 modes for axial velocity, transverse velocity, and speed of sound at $x/h=0-17$. "■" experimental and "-" Galerkin prediction.

velocity, and T_0 is the jet temperature. Initially, the calculated data is limited to the region $0<x/h<10$. The first two dominant modes are considered to obtain the time coefficients $\zeta^{(n)}$ of the dynamical equations. A system of six equations and six unknowns is solved, since the modes for u, v, and a are taken separately. The initial conditions to solve the ordinary differential equations (ODE's) are given by the first value of ζ^1 and ζ^2 at $t=0$. They are obtained from the direct projection of the first realization on the first two dominant modes. The fourth order Runge-Kutta scheme provided in MATLAB software has been utilized. For the simulation a time step of 0.5 μs was used for an accurate calculation of variables. A direct comparison between experimental data and the simulation data is shown in Fig. 9. Here, the computed values for $\zeta^{(n)}(t)$ are compared to the direct projection results for the first two modes selected. The simulation results shown in Fig. 9 for the axial and transverse velocities and the speed of sound compare reasonably well with the direct projections of realizations on the eigenfunctions. The simulation was computed to larger intervals to show the stability of the model.

The spectral content of the experimental and simulation $\zeta^{(n)}(t)$ values is shown in Fig. 10. A time length of eight periods was used in the calculation of spectra for both experimental and simulation data. The experimental data was considered as periodically repeating itself. The simulation has an oscillatory behavior with a constant frequency, however, it is not periodic because of increasing amplitude even after the initial transient. The spectra reveal that the frequency of oscillation of the simulated flow is commensurate with the experimental data. However, significant deviations are found in the amplitude of the peaks between measured and computed spectra. This may be due to the simplified equations of motion used in the simulation. In addition, the 2D (two-dimensional) model used to represent the 3D character of the real flow may have an important role. With the simplified assumptions used here, the results from the dynamical equations agree reasonably well the experimental results. Including more number of modes does not improve the results, an observation consistent with that of Rowley [19].

When the region of interest is extended up to $x/h=17$, the simulation results begin to deviate further from the POD calculations as shown in Fig. 11. This may be due to the use

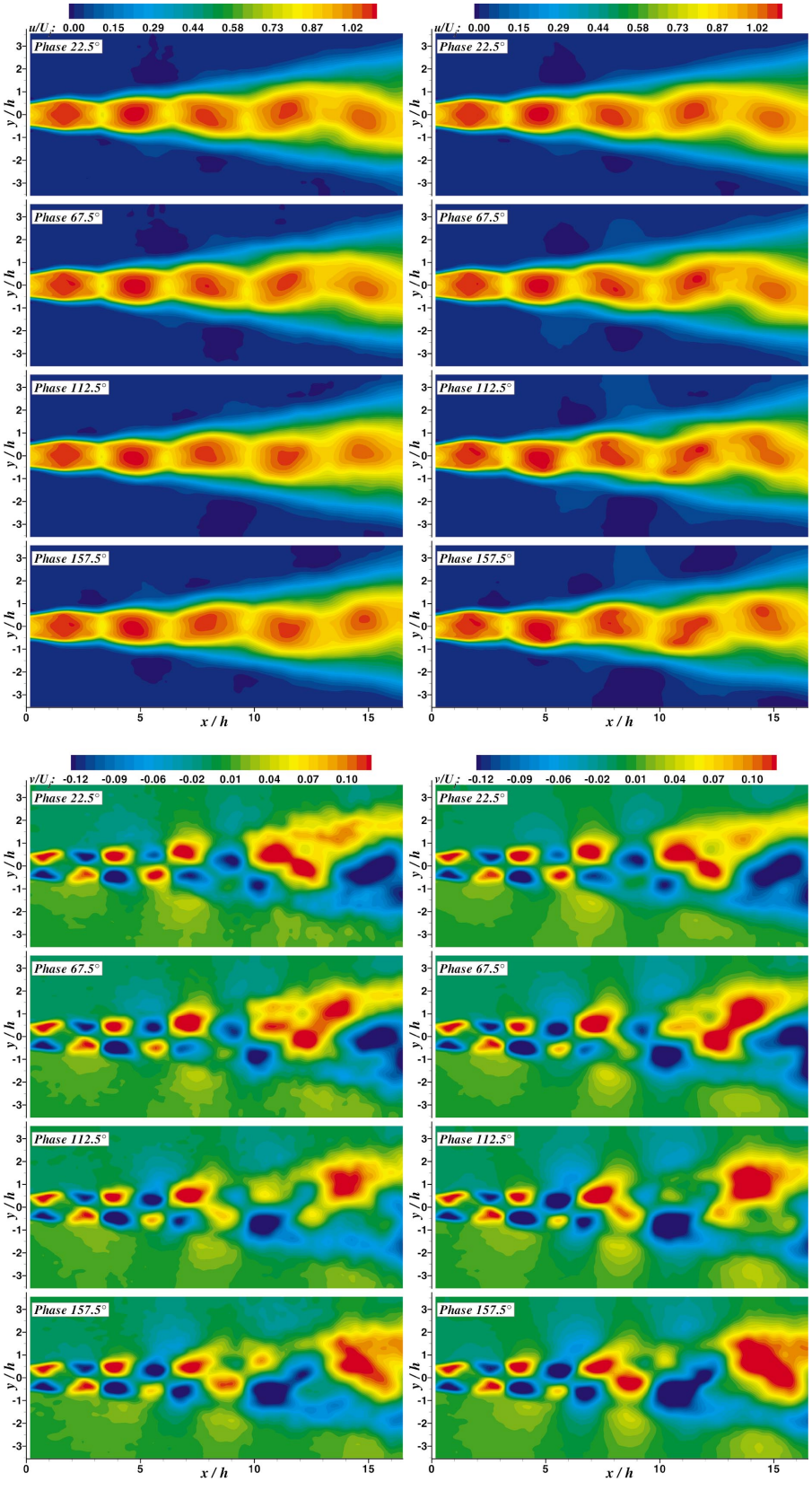

FIG. 12. (Color) Comparison of experimental flow field (left) with the results of Galerkin prediction (right), (top) axial velocity, (bottom) transverse velocity.

of isentropic Navier-Stokes equations that do not include the contributions of viscous terms, which may play an increasingly important role further downstream of the jet. Figure 12 shows comparisons between the phase-averaged experimental and simulation data for four different phases. Both the axial and transverse velocity fields are included in the figure. Although there are some differences in the details, the overall flow field is captured well in the simula-

tions. In particular, the oscillation of the jet column is captured vividly.

V. CONCLUSIONS

This work is motivated by our attempt to develop low-dimensional models to calculate supersonic jet flow fields. In general, high speed jets at relatively large Reynolds numbers show vortical structures covering a range of length scales. However, in this paper, we confine ourselves in developing a low-dimensional model for a jet that is dominated by large-scale coherent vortices. These structures are generated by a self-sustained oscillation of the jet column and are shed at a single dominant frequency making the application of the technique relatively less cumbersome.

The commonly used snapshot POD technique is used to obtain the dominant mode shapes from phase-locked instantaneous velocity fields in a selected plane of the jet in the streamwise direction. The velocity field data is obtained using the PIV technique. It was found that most of the fluctuation energy is contained within the first two modes. The reconstruction of the flow field is faithfully represented by these two modes.

A simplified version of the isentropic compressible Navier-Stokes equations is used in the analysis. The projection of the dominant POD on to these equations resulted in a low-order system of dynamical equations. Solution of this system of equations provides a description of the coherent structure dynamics associated with the eigenfunctions. The simulation results obtained using these equations compare well with the experimental results. From this study, it appears that the low order modeling of self-excited jet flows can be useful for predictions of global flow characteristics.

ACKNOWLEDGMENTS

We wish to thank the Office of Naval Research (Dr. Gabriel Roy as technical monitor) for supporting this work. The discussions with Professor Vijay Arakeri were quite useful. D.M. was partially supported by CONCYTEG and CONACYT of Mexico. We are grateful to the reviewers for their constructive comments and suggestions, which significantly improved the discussion and presentation.

[1] L. Sirovich, Q. Appl. Math. **45**, 561 (1987).
[2] J. L. Lumley, *Atmospheric Turbulence and Wave Propagation* (Nauka, Moscow, 1967).
[3] N. Aubry, P. Holmes, J. L. Lumley, and E. Stone, J. Fluid Mech. **192**, 115 (1988).
[4] D. Rempfer, Phys. Fluids **8**, 175 (1996).
[5] P. Moin and R. D. Moser, J. Fluid Mech. **200**, 471 (1989).
[6] K. S. Ball, L. Sirovich, and L. R. Keefe, Int. J. Numer. Methods Fluids **12**, 585 (1991).
[7] L. Graftieaux, M. Michard, and N. Grosjean, Meas. Sci. Technol. **12**, 1422 (2001).
[8] F. R. Payne and J. L. Lumley, Phys. Fluids **10**, 194 (1967).
[9] J. Delville, L. Ukeiley, L. Cordier, J. P. Bonnet, and M. Glauser, J. Fluid Mech. **391**, 91 (1999).
[10] M. Rajaee, S. K. F. Karlsson, and L. Sirovich, J. Fluid Mech. **258**, 1 (1994).
[11] M. N. Glauser, S. J. Leib, and W. K. George, in *Proceedings of the Fifth Symposium on Turbulent Shear Flows*, edited by F. Durst *et al.* (Springer, New York, 1987), p. 134.
[12] S. Gordeyev and F. Thomas, J. Fluid Mech. **414**, 145 (2000).
[13] J. Citriniti and W. George, J. Fluid Mech. **418**, 137 (2000).
[14] S. Bernero and E. Fiedler, Exp. Fluids **29(7)**, 274 (2000).
[15] B. Patte-Rouland, G. Lalizel, J. Moreau, and E. Rouland, Meas. Sci. Technol. **12**, 1404 (2000).
[16] B. J. Pelliccia-Kraft and D. W. Watt, Exp. Fluids **30**, 633 (2001).
[17] M. Kirby, J. P. Boris, and L. Sirovich, Int. J. Numer. Methods Fluids **10**, 411 (1990).
[18] L. Ukeiley, J. Seiner, N. Sinha, and S. Arunajatesan, Bull. Am. Phys. Soc. **45**, 138 (2000).
[19] C. W. Rowley, T. Colonius, and R. M. Murray, Sixth AIAA/CEAS Aeroacoustics Conference, Paper 2000-1969, June 2000 (unpublished).
[20] L. Ukeiley, L. Cordie, R. Manceau, J. Delville, M. Glauser, and J. Bonnet, J. Fluid Mech. **441**, 67 (2001).
[21] A. Krothapalli, M. B. Alkislar, and L. Lourenco, Seventh AIAA/CEAS Aeroacoustics Conference, Paper 2001-2144, May 2001 (unpublished).
[22] A. Powell, Aeronaut. Q. **4**, 103 (1953).
[23] A. Krothapalli, D. Baganoff, and Y. Hsia, Eighth AIAA Aeroacoustics Conference, Paper 1983-0727, April 1983 (unpublished).
[24] G. Berkooz, P. Holmes, and J. L. Lumley, Annu. Rev. Fluid Mech. **25**, 539 (1993).
[25] R. Courant and D. Hilbert, *Methods of Mathematical Physics* (Wiley, New York, 1953), Vol. 1.
[26] C. W. Rowley, Ph.D. thesis, California Institute of Technology, 2000.
[27] W. C. Reynolds and A. K. M. F. Hussain, J. Fluid Mech. **54**, 263 (1972).
[28] M. B. Alkislar, Ph.D. thesis, Florida State University, 2001.
[29] M. B. Alkislar, A. Krothapalli, and L. Lourenco, J. Visualization **3**, 135 (2000).
[30] M. B. Alkislar, A. Krothapalli, and L. Lourenco, J. Fluid Mech. **489**, 121 (2003).
[31] Palacios, G. M. Gunaratne, and M. Gorman, Chaos **7**, 463 (1997).
[32] Michalke, Prog. Aerosp. Sci. **21**, 159 (1984).